International Journal of Environment and Climate Change

Volume 14, Issue 12, Page 506-523, 2024; Article no.IJECC.122776
ISSN: 2581-8627
(Past name: British Journal of Environment & Climate Change, Past ISSN: 2231–4784)

Investigation of Mg-Doped SnO_2 Nanoparticles as an Efficient Photocatalyst for the Degradation of Crystal Violet Dye

Ruchi Bisht [a*], G.C. Joshi [b] and Chandra Shekhar Joshi [a]

[a] Department of Physics, G. B. Pant University of Agriculture and Technology, Pantnagar-263145, India.
[b] Radiations and Isotopic Tracers Laboratory (RITL), G. B. Pant University of Agriculture and Technology, Pantnagar-263145, Uttarakhand, India.

Authors' contributions

This work was carried out in collaboration among all authors. All authors read and approved the final manuscript.

Article Information

DOI: https://doi.org/10.9734/ijecc/2024/v14i124641

Open Peer Review History:
This journal follows the Advanced Open Peer Review policy. Identity of the Reviewers, Editor(s) and additional Reviewers, peer review comments, different versions of the manuscript, comments of the editors, etc are available here: https://www.sdiarticle5.com/review-history/122776

Original Research Article

Received: 25/06/2024
Accepted: 28/08/2024
Published: 24/12/2024

ABSTRACT

This study is an attempt to investigate the photocatalytic performance of magnesium (Mg) doped SnO_2 nanoparticles (NPs) for the degradation of Crystal Violet (CV) dye under sunlight irradiation. Mg doped SnO_2 NPs with varying concentrations of Mg were synthesized through coprecipitation method. The synthesized NPs were characterized using X-ray diffraction (XRD), UV-Vis spectroscopy and Fourier transform infrared (FTIR) spectroscopy to confirm their structural and optical properties. The photocatalytic efficiency of Mg-doped SnO_2 NPs was evaluated by examining the degradation rate of CV dye. The results demonstrated that Mg doping significantly

**Corresponding author: E-mail: ruchibisht956@gmail.com;*

Cite as: *Bisht, Ruchi, G.C. Joshi, and Chandra Shekhar Joshi. 2024. "Investigation of Mg-Doped SnO_2 Nanoparticles As an Efficient Photocatalyst for the Degradation of Crystal Violet Dye". International Journal of Environment and Climate Change 14 (12):506-23. https://doi.org/10.9734/ijecc/2024/v14i124641.*

improved the photocatalytic activity of SnO_2 NPs, with a 15wt% Mg doping concentration leading to the highest degradation rate of CV dye. The enhanced photocatalytic performance is attributed to the increased charge carrier separation due to Mg doping. This study highlights the potential of Mg-doped SnO_2 NPs as effective photocatalysts for the degradation of organic pollutants, offering a promising approach for wastewater treatment applications.

Keywords: Tin oxide (SnO_2); crystal violet dye; Mg-doped SnO_2 nanoparticles; doping.

1. INTRODUCTION

The discharge of waste from textiles, paper and dye industries, extensive usage and improper disposal of pesticides and fertilizers in agriculture practices have resulted in a significant rise in various organic contaminants in natural water ecosystems. Many of these organic pollutants are non-biodegradable and through anaerobic degradation they can generate carcinogenic intermediates. The textile industry consumes synthetic dyes more than 10,000 tons annually, which accounts for a fraction of 7×10^7 tons of synthetic dyes produced worldwide each year (Al-Tohamy et al., 2022). The release of these synthetic dyes into the environment causes adverse effects on human health and damages aquatic life and ecosystems (Kant, 2012). Dyes employed across various industries are categorized into cationic, anionic, and non-ionic groups based on their ionic charge. Among these dye categories, cationic dyes are considered to pose a higher level of toxicity when compared to their counterparts (Foroutan et al., 2022). Crystal violet (CV), alternatively referred to as gentian violet, methyl violet 10B, or hexamethyl pararosaniline chloride, is a cationic dye with molecular formula $C_{25}H_{30}N_3Cl$. Fig. 1. illustrates the chemical structure of the CV dye. CV dye finds widespread application in the production of printing inks, paints, and dyes for their subsequent utilization in the textile industry. Beyond serving as a biological stain and playing a central role in Gram's stain, CV dye is also frequently employed for the treatment of bacterial infection, and skin ailments in both humans and animals. Furthermore, it serves as an antifungal, antibacterial and antiparasitic component in poultry feed (Patel et al., 2021, Blanco-Flores et al., 2014). Nevertheless, extended exposure to these chemicals has been associated with certain health problems, including jaundice, mild eye discomfort, and mutagenic effects. The significant amount of these chemicals when ingested through the skin can be highly toxic to mammalian cells and can induce skin irritation and digestive track irritation, have carcinogenic properties, and may result in respiratory and kidney issues (Komal et al., 2024). These chemicals are regarded as persistent, as they are not easily digested by microorganisms (Foroutan et al., 2022; Blanco-Flores et al., 2014). Therefore, it is crucial to remove these dye pollutants from waterbodies.

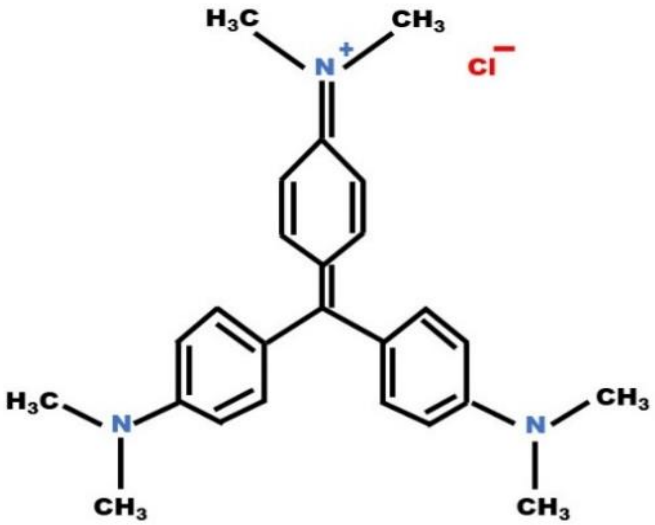

Fig. 1. Chemical structure of CV dye

Recently, researchers have been growing interest in developing highly effective semiconducting photocatalysts to eliminate organic contaminants from wastewater through light irradiation and semiconducting materials. This offers an effective and cost-efficient method for cleaning wastewater (Asaithambi et al., 2019). There are multiple techniques for dye removal, including sedimentation, chemical precipitation, adsorption, advanced oxidation processes (AOPs), ultrafiltration, reverse osmosis, ion exchange, and heterogeneous photocatalysis (Adeleke et al., 2018, Joshi et al., 2023). Recently, heterogeneous photocatalysis has become increasingly popular for dye removal due to its high efficiency and cost-effectiveness. Semiconducting metal oxides such as ZnO, TiO_2, SnO_2, Fe_2O_3, and WO_3 are often preferred materials for photocatalytic reactions (Mohammed Harshulkhan et al., 2016, Zhang et al., 2004; Kim et al., 2016; Ajeesha et al., 2021; Slimani et al., 2023; Hannachi et al., 2023; Yao et al., 2017). This preference is due to their excellent photostability, high photoactivity, biocompatibility, and the fact that they are relatively inexpensive and easy to produce. Among the different types of semiconducting metal oxides, tin oxide (SnO_2) nanostructures have garnered significant attention recently for their potential in photocatalytic applications. SnO_2 is an n-type semiconductor with a band gap energy of 3.6 eV, and it exhibits higher electron mobility compared to TiO_2 (Kar et al., 2019). Excellent transparency, high photosensitivity, chemical stability, affordability, and eco-friendliness are some of the other characteristics which makes SnO_2 an effective photocatalytic material (Ali Baig et al., 2020). However, SnO_2 faces limitations for large-scale applications due to its rapid recombination of photogenerated electron-hole pairs and low quantum yield in photocatalytic reactions, which affect its economic feasibility. Incorporating alkaline metals into the material alters the energy band gap, which can improve its electronic properties and boost its photocatalytic performance. Doping SnO_2 with alkaline metals introduces lattice defects, such as oxygen vacancies, which enhances the generation of reactive oxygen species (ROS) (Asaithambi et al., 2020). This process improves the photocatalytic efficiency of SnO_2 NPs. Appropriate metal doping can reduce the recombination of photogenerated electron-hole pairs during photocatalysis. Mg^{2+} (72 nm), with an ionic radius similar to that of Sn^{+4} (71 nm), is a promising option for doping in SnO_2 NPs (Kumari et al., 2014; Sabri et al., 2012; Xiong et al., 2016). Due to its non-toxic nature and cost-effectiveness, Mg^{2+} doping can enhance the photocatalytic properties of SnO_2 NPs. There are several chemical synthesis methods for producing SnO_2 NPs, including chemical precipitation (Sahay et al., 2013), the sol-gel process (Aziz et al., 2013), microwave technique (Krishnakumar et al., 2009), chemical co-precipitation (Asaithambi et al., 2020) and hydrothermal method (Patil et al., 2012; Bala Narsaiah et al., 2024). The chemical co-precipitation method is highly beneficial for synthesizing nanomaterials because it offers a simple and cost-effective way to consistently produce NPs with controlled sizes and specific shapes (Tazikeh et al., 2014).

In this study, we extensively explore the photocatalytic activity of SnO_2 NPs that are doped with alkaline earth metal Mg. These NPs were synthesized using a straightforward co-precipitation method. The investigation covered the structural, optical and compositional characteristics of both undoped and alkaline metal-doped SnO_2 NPs. Additionally, the study includes a detailed analysis and discussion of the photocatalytic efficiency of these NPs.

2. MATERIALS AND METHODS

2.1 Materials Used

Tin (IV) Chloride Pentahydrate ($SnCl_4.5H_2O$), Magnesium Nitrate Hexahydrate (Mg $(NO_3)_2{\cdot}6H_2O$), Sodium Hydroxide (NaOH) pellets, and Polyethylene Glycol (PEG), were used as reagent in this experiment. All these chemicals of Analytical Reagent (AR) grade were purchased from Hi-media and used directly without any further purification. Double distilled water was used for all experimental procedures.

2.2 Synthesis of Mg-Doped SNO_2 NPs

Homogeneous solutions of stannic chloride pentahydrate and appropriate amount (5 wt%, 10 wt% and 15 wt%) of magnesium nitrate hexahydrate (Mg $(NO_3)_2{\cdot}6H_2O$) in 50 ml of DI water were prepared separately. After 15 minutes of stirring, the solution containing magnesium nitrate hexahydrate was mixed with the tin (II) chloride pentahydrate and subsequently, 5 ml PEG was added to the resulting mixture. The mixture was further stirred for another 30 min and thereafter, 0.5M NaOH solution was added dropwise until the pH

reached upto 12. The resulting mixture was then stirred for an additional 2 hours at 60°C. After completion of reaction, a thick off-white precipitate was formed at the bottom of the flask. The precipitate was collected and thoroughly rinsed with deionized water and ethanol to eliminate any impurities. The precipitate was dried at 60°C in a hot air oven for 10 hours. After drying, it was collected and ground using a mortar and pestle. The resulting powder was then placed in a crucible and calcinated at 450°C for 2 hours in a muffle furnace. After calcination tin oxide NPs were obtained. Pure and Mg-doped SnO_2 NPs are named as SM0, SM5, SM10 and SM15, where 0, 5, 10, and 15 represent the weight percentage of Mg in Mg-doped SnO_2 NPs.

2.3 Characterization Techniques

The purity, crystalline phase, and structure of synthesized NPs were analyzed using X-ray diffraction (XRD) with a Bruker D8-Advance diffractometer equipped with Cu Kα radiation (λ = 0.15418 nm. Fourier transform infrared (FTIR) spectra were recorded on an Alpha 200855 FTIR system. Optical properties were studied using UV-Vis spectrophotometer (LAMBDA 365, PerkinElmer) to measure absorbance.

2.4 Photocatalytic Degradation Experiment

The photocatalytic performance of the synthesized pure and Mg-doped SnO_2 NPs was evaluated by analyzing the degradation of crystal violet (CV) dye at a concentration of 10 mg/L under solar irradiation. The photocatalytic degradation of all the samples was examined by dispersing 20 mg catalyst in 100 ml dye solution. Before exposing the CV/photocatalyst solution to sunlight, the solutions were magnetically stirred for 1 hour at room temperature to attain adsorption-desorption equilibrium. After confirming the adsorption-desorption equilibrium, the photocatalysis was initiated by irradiating the CV/photocatalyst solution to sunlight. The dye degradation was tracked by periodically taking 2 ml samples from the suspension and measuring their absorbance. The absorption spectra were recorded using UV–VIS spectrometer after centrifugation was performed to eliminate the suspended catalyst particles from the suspension. A UV–Visible spectrophotometer was employed to monitor how the concentration of CV dye changed over time. The CV solution were placed back into the beaker to maintain a consistent volume of the dye solutions after measuring the absorbance at each time point. The kinetics of CV photodegradation was studied using a pseudo-first-order kinetic equation (1) derived from the Langmuir-Hinshelwood model (Khairy & Zakaria, 2014):

$$ln(C_o/C_t) = kT \quad (1)$$

where C_O is the initial concentration of the dye (0 min), and C_t is the concentration of dye at time t. The rate constant, k, or equilibrium constant, is determined by analyzing the slope of the graph that plots $ln(C_o/C_t)$ against reaction time (t), according to relation (2) (Abraham et al., 2016):

$$k = 2.303 \times slope \quad (2)$$

The percentage efficiency (R %) of a photocatalyst, was determined utilizing Equation (3) (Senthil Kumar et al., 2015):

$$\text{Degradation efficiency \%} = \left(\frac{C_O - C_t}{C_o}\right) \times 100 \quad (3)$$

This formula expresses the efficiency as a percentage by comparing the reduction in contaminant concentration to the initial amount.

3. RESULTS AND DISCUSSION

3.1 Structural Analysis

Fig. 2 shows the XRD patterns of pure and Mg (5, 10 and 15 wt.%) doped SnO_2 NPs. All the samples are indexed with the tetragonal rutile phase of SnO_2. The diffraction peaks observed correspond to the (110), (101), (200), (211), (002), (310), (112), (202), (321) and (222) crystalline planes of the cassiterite phase of tetragonal SnO_2 at 2θ values of 26.69, 33.87, 38.01, 51.97, 57.93, 61.76, 65.38, 71.67, 78.61 and 84.01, respectively. These planes are aligned with the standard JCPDS card number 41-1445 (Kim et al., 2016). The average crystallite sizes (D) of the synthesized samples were determined using the Scherrer equation (Manjula & Selvan, 2017) (4):

$$D = \frac{k\prime\lambda}{\beta Cos\theta} \quad (4)$$

The constant k' is Scherrer constant or particle shape factor k having value 0.9, while λ represents the X-ray wavelength, which is 0.154 nm. The variables β and θ are full width at half maximum (FWHM) and diffraction angle, respectively. The absence of Mg peak in the XRD pattern could be attributed to the effective dispersion of Mg within the SnO_2 NPs, as well as the low concentration of Mg.

Microstrain (ε), lattice parameters 'a=b' and 'c' and lattice strain (δ) was determined using the following equations (5-7) (Madiba et al., 2017; Mirzayev et al., 2018; Sudha et al., 2016):

$$\varepsilon = \frac{\beta}{4\tan\theta} \quad (5)$$

$$\frac{1}{d^2} = \frac{h^2+k^2}{a^2} + \frac{l^2}{c^2} \quad (6)$$

$$\delta = \frac{1}{D^2} \quad (7)$$

Where h, k, and l represent the Miller indices, a=b and c are the lattice parameters, and d denotes the interplanar spacing. The average crystallite size, exhibited a slight variation when Mg was doped under the same experimental conditions. The decrease in crystallite sizes upon doping is attributed to the distortion caused in the SnO_2 lattice by the incorporation of Mg^{2+} ions. This distortion reduces nucleation and impedes the growth rate of SnO_2 crystal grains (Lavanya et al., 2012). Moreover, lattice parameters show no significant change, likely because the Mg^{+2} dopant ion (72 nm) is nearly the same size as the host Sn^{+4} ion (71 nm). The structural parameters of pure and Mg-doped SnO_2 NPs are given in Table 1.

3.2 Fourier Transform Infrared (FTIR) Analysis

Fig. 3 presents the FTIR spectra for both pristine and Mg-doped SnO_2 NPs, recorded over the wavenumber range of 400 to 4000 cm^{-1} after the sample powder was diluted with KBr. The broad and intense band in the range of 3000–3600 cm^{-1} are the characteristic of stretching vibrational modes of O–H bond, which are attributed to the Sn-OH groups and adsorbed water molecules (Farrukh et al., n.d.; Pascariu et al., 2016). The peaks observed around 1643 cm^{-1} correspond to the O-H bending vibrations are associated with residual water molecules used during mixing of KBr binder for measurement (Nachiar & Muthukumaran, 2019). The feeble band observed at 2329 cm^{-1} might be attributed to the absorption of CO_2 from ambient air atmosphere (Jouhannaud et al., 2008). The symmetric and asymmetric C–H vibrations were observed at 2967 cm^{-1} and 2863 cm^{-1}, respectively. This implies that the NPs are essentially capped with the ethylene glycol used in their synthesis (Nachiar & Muthukumaran, 2019; Singh et al., 2014). The prominent absorption bands observed in the lower-wavenumber region (400–800 cm^{-1}), particularly at 502 and 612 cm^{-1}, are characteristic IR fingerprints of the doped SnO_2 NPs. These bands correspond to anti-symmetric O–Sn–O vibrations and the Sn–O (terminal oxygen vibration of Sn–OH) lattice-extending vibrations, respectively (Manjula & Selvan, 2017; Dobrucka et al., 2018). Furthermore, the bands detected around 1379 cm^{-1} are ascribed to the bending vibrations of the C=O bond (Zhou et al., 2018).

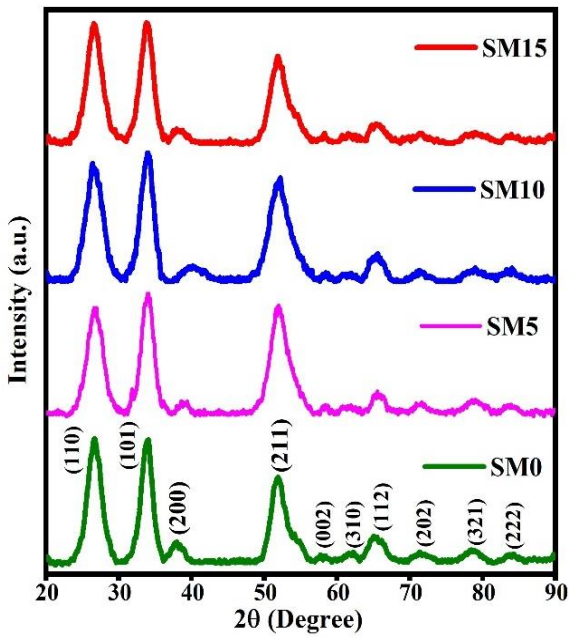

Fig. 2. X-ray diffraction of pure SnO_2 and SnO_2: Mg NPs.

Table 1. The structural parameters of Un-doped and Mg-doped SnO_2 NPs.

Sample	(hkl)	2θ(°)	β (×10^{-3}) rad	Average crystallite size D (nm)	δ (×10^{-2}lines nm^{-2})	ε (×10^{-3})	Lattice constants (Å)	
							a	c
SM0	110	26.69	0.0332	4.49	5.437	0.0350	4.7404	3.1929
	101	33.87	0.0266		3.388	0.0219		
SM5	110	26.75	0.0375	4.39	6.951	0.0395	4.7369	3.1859
	101	33.95	0.0292		4.081	0.0239		
SM10	110	26.65	0.0406	3.80	8.147	0.0429	4.7212	3.1962
	101	33.91	0.0304		4.413	0.0249		
SM15	110	26.66	0.0361	3.72	6.421	0.0380	4.6885	3.1797
	101	33.87	0.0304		4.422	0.0250		

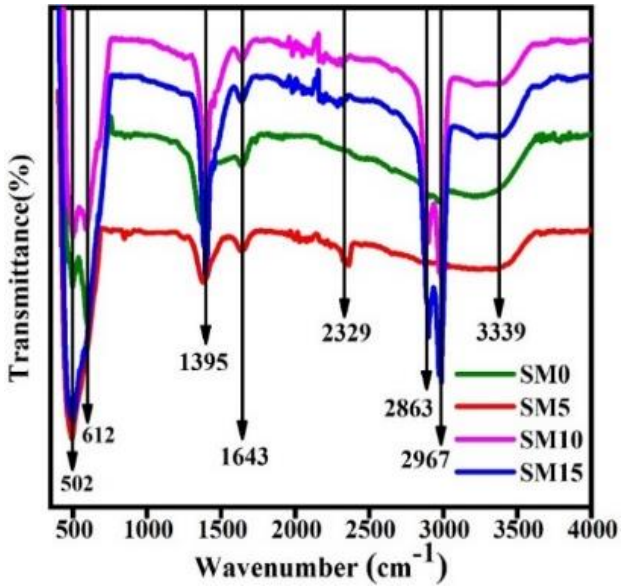

Fig. 3. FTIR spectra of pure and Mg-doped SnO_2 NPs.

Table 2. Absorption band position along with corresponding assigned functional groups in samples

Absorption bands (~ cm^{-1})	Functional group	Reference
473	Sn-O stretching mode of vibration	(Manjula & Selvan, 2017; Dobrucka et al., 2018)
607	O-Sn-O stretching mode of vibration	(Manjula & Selvan, 2017; Dobrucka et al., 2018)
1379	C=O bond stretching vibration	(Zhou et al., 2018)
1637	Bending vibration of surface hydroxyl (-OH) groups	(Kumar et al., 2015)
2863	Asymmetric vibration attributed to C-H bonds	(Singh et al., 2014)
2967	Symmetric vibration attributed to C-H bonds	(Nachiar & Muthukumaran, 2019; Singh et al., 2014)
3332	Stretching vibration of surface hydroxyl (-OH) groups	(Kumar et al., 2015)

However, no specific peaks corresponding to Mg–O bonds were observed, indicating the incorporation of Mg into the SnO_2-structured matrix as observed in the XRD analysis. A minor variation is noticed in the intensity and position of these characteristic bands. This effect is due to the larger ionic radii of alkaline metal ions Mg^{2+} compared to Sn^{4+}, which alters the SnO_2 lattice. Additionally, these dopant ions may occupy interstitial sites, contributing to shift in the IR absorption spectrum (Asaithambi et al., 2020). Absorption band position along with corresponding assigned functional groups in samples are given. In Table 2.

3.3 Optical Studies

Fig. 4 (a) represents the optical absorption spectra for pure and Mg-doped SnO_2 NPs recorded in the range of 300 to 800 nm. Absorbance is expected to be influenced by various factors, including band gap, oxygen deficiency, surface roughness, and impurity centers (Ahmed et al., 2011). The absorption edge of various samples varies with the concentration of Mg in SnO_2 NPs. As the Mg content increases in the SnO_2 host, a noticeable shift towards lower wavelengths (blue shift) is observed in the absorption edge which may lead to an increment in band gap.

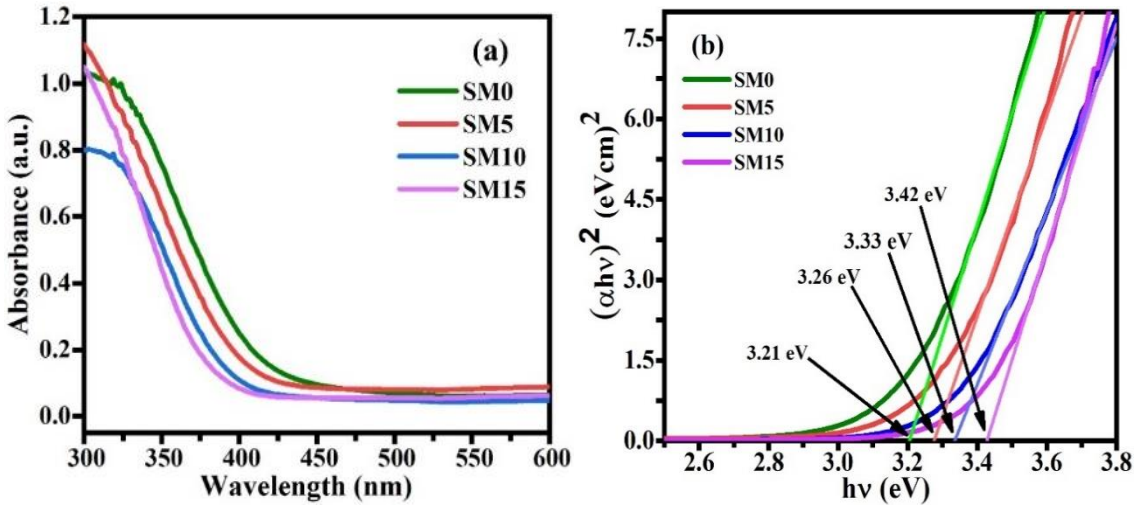

Fig. 4. (a) UV-visible absorption spectra and (b) Tauc's plot of pure and Mg-doped SnO_2 NPs.

The optical bandgap of pure and Mg-doped SnO_2 NPs were determined using Tauc plots method equation (Asaithambi et al., 2019) (8):

$$(\alpha h\nu) = B(h\upsilon - E_g)^n \quad (8)$$

Here, α represents the absorption coefficient, B is a constant, v denotes frequency, h stands for Planck's constant, and Eg represents the bandgap energy. The parameter n equals ½ specifically for the direct bandgap of the semiconductor.

The optical band gap (E_g) can be determined by extrapolating linear region of a plot of $(\alpha hv)^2$ vs hv. Fig. 4(b) graphically represents the plot of $(\alpha hv)^2$ versus hv for the synthesized SnO_2 NPs. The measured band gap values for Mg-doped SnO_2 with doping concentrations of 0%, 5%, 10%, and 15% are 3.21 eV, 3.26 eV, 3.33 eV, and 3.42 eV, respectively. The results showed that doping Mg led to an increase in the band gap energy of pure SnO_2 resulting in a blue shift. The rise in the band-gap suggested that Mg was effectively integrated into the SnO_2 crystal structure. The observed rise in Eg could be attributed to the quantum confinement effect (Mohana Priya et al., 2016). Moreover, observed increase in the band gap with an increase in Mg doping can be attributed to the dominance of d-d transitions over sp-d transitions (Nyamukamba et al., 2017).

3.4 Photocatalytic Degradation Studies

The synthesized pure and Mg-doped SnO_2 NPs were employed as photocatalysts for the degradation of CV dye under solar irradiation. The absorption of CV dye was measured using UV–Visible spectrophotometer. The UV–Visible spectra for the CV dye solutions degraded by synthesized samples as a photocatalyst are displayed in Fig. 5.

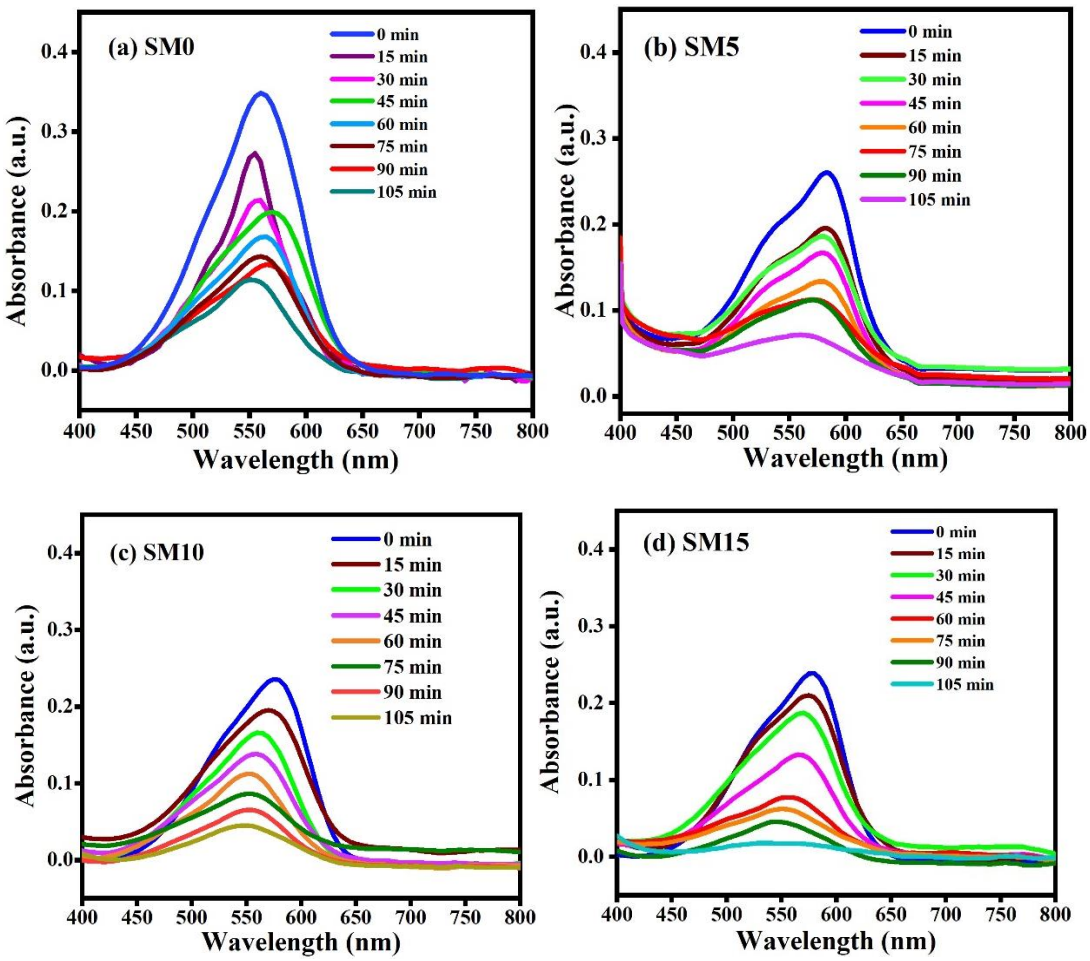

Fig. 5. UV-Vis absorption spectra of CV dye for (a) SM0, (b) SM5, (c) SM10, and (d) SM15 photocatalyst.

Table 3. Band gap, Rate constant (k) and linear regression coefficient R^2 values of the photocatalyst

Samples	Band gap E_g (eV)	Irradiation time (min)	Degradation efficiency (%)	Rate constant K (min^{-1})	R^2
SM0	3.21	105	67	0.02073	0.97
SM5	3.26	105	72	0.02464	0.95
SM10	3.33	105	81	0.03385	0.96
SM15	3.42	105	93	0.05527	0.91

The change in dye concentration with time of reaction for pure and Mg-doped SnO_2 NPs is depicted in Fig. 6 (a). From Fig. 6(a), it can be observed that highest effectiveness is achieved by the SM15 photocatalyst. The dye degradation process follows pseudo-first-order kinetics. The graph for pseudo-first-order kinetics is plotted with ln (C_O/C_t) against the reaction time for each of the synthesized photocatalysts. Fig. 6 (b) represents the pseudo-first-order kinetic plots for all the samples. The linearity observed in the plots for all the samples suggested that pseudo-first-order kinetics are applicable. The enhanced photocatalytic performance is attributed to a larger surface area, the availability of more reactive ions, and an increase in active sites.

The rate constant for the degradation reactions of the synthesized photocatalysts were determined using equation (2). The rate constants calculated for the degradation of CV dye are plotted against the synthesized photocatalyst, as illustrated in Fig. 7 (a). The calculated values of rate constants are 0.02073, 0.02464, 0.03385 and 0.0552 for SM0, SM5, SM10 and SM15, respectively. Table 3. shows the linear regression coefficient (R^2), reaction rate constant (k), and percentage of degradation efficiency for each sample for the degradation process of CV dye.

The degradation of the CV dye under solar light exposure, using 10 mg of the prepared photocatalysts, is illustrated in Fig. 7(b) by plotting the efficiency of degradation as a function of reaction time. SM15 photocatalyst shows maximum degradation efficiency of 93% over time of 105 min whereas SM0 photocatalyst possesses degradation efficiency of merely 67%. The low efficiency of pure SnO_2 can be attributed to the rapid recombination of charge carriers. This rapid recombination reduces the probability of the movement of the photo-generated charge carriers reaching the catalyst surface, which solar light in turn diminishes photocatalytic activity (Maleki et al., 2015; Kumar et al., 2017).

The findings indicated that 15 wt% Mg-doped SnO_2 photocatalysts exhibit outstanding photocatalytic performance in breaking down CV dye. The enhancement in photocatalytic performance resulting from Mg doping can be linked to a blue shift, which is explained by the Burstein–Moss effect (Karthikeyan & Pandiyarajan, 2010). The Fermi level in Mg-doped SnO_2 NPs may be positioned at a higher energy level, causing a shift in the absorption edge towards shorter wavelengths. A larger band gap energy is associated with a higher redox potential of electron-hole pairs, which in turn leads to enhanced photocatalytic activity. Similar results are reported by Behnajady & Tohidi, (2014). Also based on the XRD results of this study, the reduction in crystallite size leads to an increased surface-to-volume ratio, which significantly improves the photocatalytic capabilities (Bindu & Thomas, 2014). It is important to note that a material with lower band gap doesn't necessarily exhibit higher photocatalytic activity as might be expected. The photocatalytic performance of SM0 photocatalyst with calculated band gap of 3.21 eV was surprisingly lower than that of SM15 photocatalyst, which had band gap of 3.42 eV, despite expectations based on their band gap values. This observation indicated that narrowing the band gap can enhance the absorption of light, although it does not necessarily lead to improved photocatalytic activity under visible light conditions. This suggested that factors beyond band gap narrowing may influence the photocatalytic activity of SnO_2 NPs. These factors may include rate of electron-hole recombination, hydrophilicity, and variations in surface area and surface properties that can enhance adsorption. Table 4. Presents a comparative analysis of our study alongside other recent research on the degradation of CV dye using various photocatalysts.

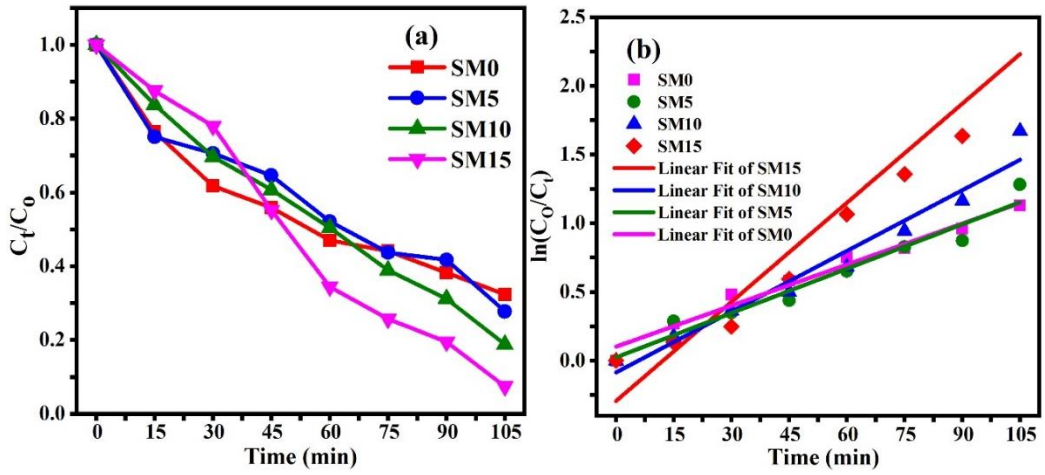

Fig. 6. (a) Relative concentration vs time plot of CV dye (b) Pseudo first-order kinetics for the degradation of CV dye for different catalysts

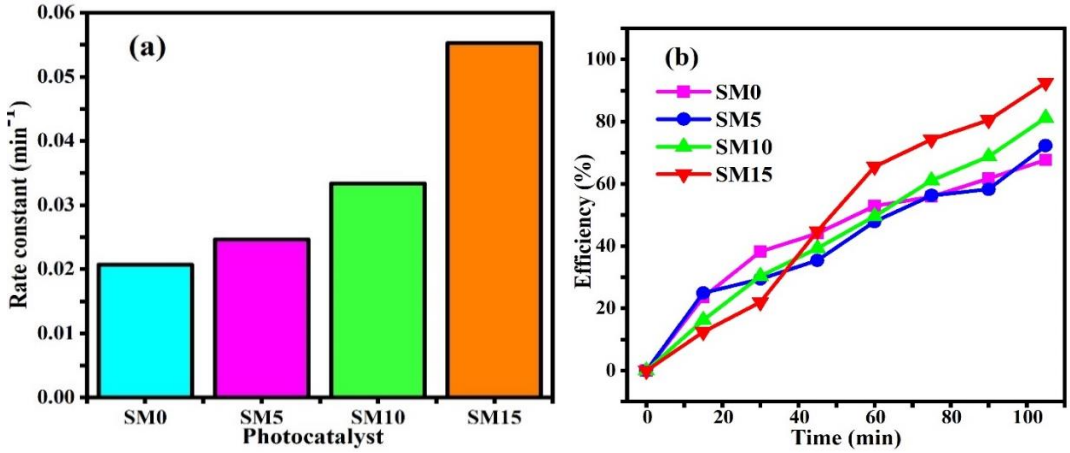

Fig. 7. (a) Representation of rate constant through Histogram (b) Time-dependent degradation efficiency of the samples

3.5 Photocatalytic Degradation Mechanism

Fig 8. illustrates the process of photocatalytic degradation of CV dye employing Mg-doped SnO_2 photocatalyst. When exposed to sunlight, SnO_2 can absorb photons causing an electron to move from the valence band to the conduction band (Kumar et al., 2017). Generally, these electron-hole pairs tend to recombine rapidly, leaving insufficient time for them to engage in any catalytic reaction (Sharma et al., 2019). The recombination of electron-hole pairs can be reduced, by incorporating Mg into SnO_2 NPs. Hence, electrons and holes move more efficiently to the surface of catalyst, where they engage in redox reactions with adsorbed species. The isolated holes in the valence band (VB) of SnO_2 can interact with water molecules to produce hydroxyl radicals. At the same time, the electrons that are captured by Mg ions are transferred to oxygen molecules, leading to the formation of reactive superoxide radicals (Sadhanala et al., 2018). These superoxide radicals are then converted into hydroxyl radicals through multiple electron reduction steps, as described in Equations (9-14). The reactive radicals produced may partially or entirely oxidize organic pollutants, transforming them into harmless substances or degraded products i.e., CO_2 and H_2O. This proposed mechanism is depicted in Fig. 8, which illustrates the potential degradation process of organic pollutants under sunlight exposure. The reaction mechanism for the photocatalytic degradation of CV dye in the presence of sunlight can be described as follows (Ahmed et al., 2019):

Table 4. Comparison of photocatalytic activity of present work with other nanomaterials for the degradation of different organic dyes

Photocatalyst	Dose (mg)	Dye	Dye concentration (mg/l)	Light source	Degradation time (min)	Degradation Efficiency (%)	References
Mg-doped CuFeO2	50	Methylene Blue (MB)	50 ppm (50 ml)	Visible light source.	90	92.7	(Chang et al., 2021)
ZnO	150	Crystal Violet (CV)	10 (100 ml)	UV irradiation	120	90	(Franco et al., 2019)
Gd doped BFO	200	Crystal Violet (CV)	20	Mercury lamp 250 W	105	84.5	(Kossar et al., 2021)
Mg-doped ZnO	200	Methylene blue (MB)	10^{-5} M (200 mL)	Xenon lamp	60	99	(Sa-nguanprang et al., 2019)
Titanate nanosheets (TNT)	20	Crystal Violet (CV)	200 (20ml)	UV lamp 16 W	75	100	(Rashad et al., 2019)
Mg-doped TiO_2	100	Methylene orange (MO)	10 (100 ml)	UV light	120	47.82	(Athira et al., 2020)
N doped SnO_2	100	Crystal Violet (CV)	20×10^{-6} M (100 ml)	UV Light irradiation	90	73	(Bhawna et al., 2023)
Glutamine-assisted SnO_2 nanorods	10	Crystal Violet (CV)	20 (100 ml)	Mercury lamp 250W	60	97.3	(Alharbi et al., 2022)
Mg-doped CuFeO2	50	Methylene Blue (MB)	50 ppm (50 ml)	Visible light source.	90	92.7	(Chang et al., 2021)
$SrFe_2O_4$	50	Crystal Violet (CV)	10 (50 ml)	Microwave irradiation	10	88.6	(Liu et al., 2018)
Mg-doped ZnO	50	Rhodamine B (RhB)	20 ppm (150 ml)	UV 125 W	120	78	(Pradeev raj et al., 2018)
$BaFe_2O_4$	50	Crystal Violet	10 (50 ml)	Microwave irradiation	10	96.6	(Liu et al., 2016)
Mg-doped CuO	200	Methylene Blue (MB)	20 μM (300 mL)	UV Hg lamp 450 W	180	95.71	(Azharudeen et al., 2022)
Sn@C-dots/TiO2 t	60	Crystal Violet (CV)	(100 ml)	Sunlight	210	60	(Kumar et al., 2017)
Mg-doped CeO_2	10	Methylene Blue (MB) dye	20 ppm (200 ml)	UV (20 W)	120	75.2	(Murugan et al., 2018)

Photocatalyst	Dose (mg)	Dye	Dye concentration (mg/l)	Light source	Degradation time (min)	Degradation Efficiency (%)	References
MoS_2 NFs	20	Crystal Violet (CV)	0.1 (100 ml)	Sunlight	40	99.3	(Alharbi et al., 2022)
SM0	20	Crystal Violet (CV)	10 (100 ml)	Sunlight	105	67	This work
SM5	20	Crystal Violet (CV)	10 (100 ml)	Sunlight	105	72	This work
SM10	20	Crystal Violet (CV)	10 (100 ml)	Sunlight	105	81	This work
SM15	20	Crystal Violet (CV)	10 (100 ml)	Sunlight	105	93	This work

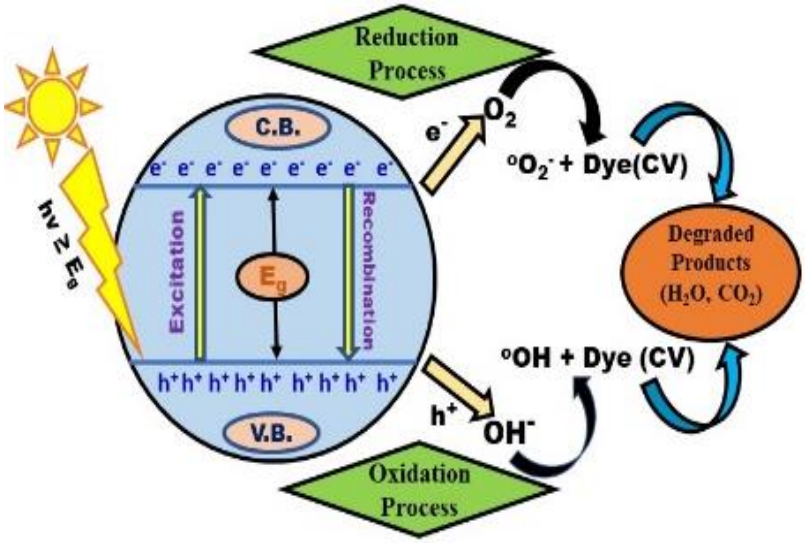

Fig. 8. Mechanism of Mg-doped SnO_2 NPs Facilitated Photocatalytic Breakdown of Crystal Violet (CV) Dye

$$\mathrm{Mg-SnO_2} + h\nu \longrightarrow Mg - SnO_2 + e^-_{(CB)} + h^+_{(VB)} \quad (9)$$

$$Mg - SnO_2 + e^-_{(CB)} + O_2 \longrightarrow {}^{o}O_2^- \quad (10)$$

$${}^{o}O_2^- + e^- + 2H^+ \rightarrow H_2O_2 \quad (11)$$

$$H_2O_2 + e^- \longrightarrow {}^{\circ}OH + OH^- \quad (12)$$

$$\mathrm{Mg-SnO_2} + h^+_{(VB)} + H_2O \longrightarrow H^+ + {}^{\circ}OH \quad (13)$$

$$\text{Organic pollutant} + {}^{\circ}OH \longrightarrow degraded\ products \quad (14)$$

4. CONCLUSION

Pure and Mg-doped SnO_2 NPs were synthesized using the chemical co-precipitation method and used as a photocatalyst to degrade Crystal Violet (CV) dye under sunlight irradiation. The XRD analysis reveals that the nanoparticles possess an average size of 4-3 nm and exhibit tetragonal rutile phase of SnO_2. The FTIR spectra validated the synthesis of Mg-doped SnO_2 NPs, indicating the presence of both Sn-O-Sn and Sn-O bands. The band gap of the samples was explored using UV-visible absorption spectroscopy, revealing an increment in band gap from 3.21 eV for undoped (SM0) to 3.42 eV for 15 wt% (SM15) Mg-doped SnO_2 NPs. Among the tested samples, 15 wt% SnO_2 sample exhibited the most effective photocatalytic activity. The study revealed that a photocatalyst with a lower band gap does not necessarily exhibit superior photocatalytic activity compared to wide band gap photocatalysts under visible light irradiation, contrary to what might be anticipated. Other factors like surface area, electron-hole recombination and hydrophilicity can surpass band gap narrowing in boosting the overall efficiency of the photocatalyst. This research could offer novel perspectives on the development of semiconducting metal oxide nanoparticles with potential applications in photocatalysis.

DISCLAIMER (ARTIFICIAL INTELLIGENCE)

Author(s) hereby declare that NO generative AI technologies such as Large Language Models (ChatGPT, COPILOT, etc) and text-to-image generators have been used during writing or editing of manuscripts.

ACKNOWLEDGEMENT

The authors would like to acknowledge that this research was conducted without any specific grant from funding agencies.

COMPETING INTERESTS

Authors have declared that no competing interests exist.

REFERENCES

Abraham, D. S., David, S. T., Bennie, R. B., et al. (2016). Eco-friendly and green synthesis of $BiVO_4$ nanoparticle using microwave irradiation as photocatalyst for the degradation of Alizarin Red S. *Journal of Molecular Structure, 1113*, 174–181.

https://doi.org/10.1016/j.molstruc.2016.01.053

Adeleke, J. T., Theivasanthi, T., Thiruppathi, M., et al. (2018). Photocatalytic degradation of methylene blue by $ZnO/NiFe_2O_4$ nanoparticles. *Applied Surface Science, 455*, 195–200. https://doi.org/10.1016/j.apsusc.2018.05.184

Ahmed, A. S., Shafeeq, M. M., Singla, M. L., et al. (2011). Band gap narrowing and fluorescence properties of nickel doped SnO_2 nanoparticles. *Journal of Luminescence, 131*, 1–6. https://doi.org/10.1016/j.jlumin.2010.07.017

Ahmed, A., Naseem Siddique, M., Alam, U., et al. (2019). Improved photocatalytic activity of Sr doped SnO_2 nanoparticles: A role of oxygen vacancy. *Applied Surface Science, 463*, 976–985. https://doi.org/10.1016/j.apsusc.2018.08.182

Ajeesha, T., A. A., George, M., et al. (2021). Nickel substituted $MgFe_2O_4$ nanoparticles via co-precipitation method for photocatalytic applications. *Physica B: Condensed Matter, 606*, 412660. https://doi.org/10.1016/j.physb.2020.412660

Alharbi, A., Shah, R. K., Sayqal, A., et al. (2022). Facile hydrothermal synthesis of glutamine-assisted tin oxide nanorods for efficient photocatalytic degradation of crystal violet dye. *International Journal of Environmental Analytical Chemistry, 102*, 7647–7658. https://doi.org/10.1080/03067319.2020.1836172

Ali Baig, A. B., Rathinam, V., & Palaninathan, J. (2020). Photodegradation activity of yttrium-doped SnO_2 nanoparticles against methylene blue dye and antibacterial effects. *Applied Water Science, 10*, 1143. https://doi.org/10.1007/s13201-020-1143-1

Al-Tohamy, R., Ali, S. S., Li, F., et al. (2022). A critical review on the treatment of dye-containing wastewater: Ecotoxicological and health concerns of textile dyes and possible remediation approaches for environmental safety. *Ecotoxicology and Environmental Safety, 231*, 113175. https://doi.org/10.1016/j.ecoenv.2022.113175

Asaithambi, S., Murugan, R., Sakthivel, P., et al. (2019). Influence of Ni doping in SnO_2 nanoparticles with enhanced visible light photocatalytic activity for degradation of methylene blue dye. *Journal of Nanoscience and Nanotechnology, 19*, 4438–4446. https://doi.org/10.1166/jnn.2019.16493

Asaithambi, S., Sakthivel, P., Karuppaiah, M., et al. (2019). Preparation of SnO_2 nanoparticles with addition of Co ions for photocatalytic activity of brilliant green dye degradation. *Journal of Electronic Materials, 48*, 2183–2194. https://doi.org/10.1007/s11664-019-07061-5

Asaithambi, S., Sakthivel, P., Karuppaiah, M., et al. (2020). Improved photocatalytic performance of nanostructured SnO_2 via addition of alkaline earth metals (Ba^{2+}, Ca^{2+} and Mg^{2+}) under visible light irradiation. *Applied Physics A: Materials Science & Processing, 126*, 3441–3448. https://doi.org/10.1007/s00339-020-3441-8

Asaithambi, S., Sakthivel, P., Karuppaiah, M., et al. (2020). Investigation of electrochemical properties of various transition metals doped SnO_2 spherical nanostructures for supercapacitor applications. *Journal of Energy Storage, 31*, 101530. https://doi.org/10.1016/j.est.2020.101530

Athira, K., Merin, K. T., Raguram, T., & Rajni, K. S. (2020). Synthesis and characterization of Mg doped TiO_2 nanoparticles for photocatalytic applications. *Materials Today: Proceedings, 2321–2327*. Elsevier Ltd.

Azharudeen, A. M., Badhusha, A. M. I., Khan, M. S., et al. (2022). Solar power light-driven improved photocatalytic action of Mg-doped CuO nanomaterial modified with polyvinyl alcohol. *Journal of Nanomaterials, 2022*, Article 2430840. https://doi.org/10.1155/2022/2430840

Aziz, M., Saber Abbas, S., & Wan Baharom, W. R. (2013). Size-controlled synthesis of SnO_2 nanoparticles by sol-gel method. *Materials Letters, 91*, 31–34. https://doi.org/10.1016/j.matlet.2012.09.079

Bala Narsaiah, R. L., Justin, P., & et al. (2024). Enhanced performance of hydrothermally synthesized zinc vanadium oxide nanoparticles for supercapacitor and photocatalytic applications. *Journal of the Indian Chemical Society, 101*, 101247. https://doi.org/10.1016/j.jics.2024.101247

Behnajady, M. A., & Tohidi, Y. (2014). Synthesis, characterization and photocatalytic activity of Mg-impregnated $ZnO\text{-}SnO_2$ coupled

nanoparticles. *Photochemistry and Photobiology, 90*, 51–56. https://doi.org/10.1111/php.12164

Bhawna, Sharma, R., Kumar, S., et al. (2023). Unlocking the potential of N-doped SnO_2 for sustainable photocatalytic degradation of carcinogenic dyes. *Separations, 10*, Article 322. https://doi.org/10.3390/separations10060322

Bindu, P., & Thomas, S. (2014). Estimation of lattice strain in ZnO nanoparticles: X-ray peak profile analysis. *Journal of Theoretical and Applied Physics, 8*, 123–134. https://doi.org/10.1007/s40094-014-0141-9

Blanco-Flores, A., Colín-Cruz, A., Gutiérrez-Segura, E., et al. (2014). Efficient removal of crystal violet dye from aqueous solutions by vitreous tuff mineral. *Environmental Technology, 35*, 1508–1519. https://doi.org/10.1080/09593330.2013.871352

Chang, Y. H., Wang, H., Siao, T. F., et al. (2021). A new solution route for the synthesis of $CuFeO_2$ and Mg-doped $CuFeO_2$ as catalysts for dye degradation and CO_2 conversion. *Journal of Alloys and Compounds, 854*, Article 157235. https://doi.org/10.1016/j.jallcom.2020.157235

Dobrucka, R., Dlugaszewska, J., & Kaczmarek, M. (2018). Cytotoxic and antimicrobial effect of biosynthesized SnO_2 nanoparticles using *Prunus spinosae* flos extract. *Inorganic and Nano-Metal Chemistry, 48*, 367–376. https://doi.org/10.1080/24701556.2019.1569054

Farrukh, M. A., Rahman, I. A., & Adnan, R. (n.d.). Synthesis and characterization of high surface area tin oxide nanoparticles via the sol-gel method as a catalyst for the hydrogenation of styrene.

Foroutan, R., Peighambardoust, S. J., Boffito, D. C., & Ramavandi, B. (2022). Sono-Photocatalytic activity of Cloisite 30B/ZnO/Ag_2O nanocomposite for the simultaneous degradation of crystal violet and methylene blue dyes in aqueous media. *Nanomaterials, 12*(18), 3103. https://doi.org/10.3390/nano12183103

Franco, P., Sacco, O., De Marco, I., & Vaiano, V. (2019). Zinc oxide nanoparticles obtained by supercritical antisolvent precipitation for the photocatalytic degradation of crystal violet dye. *Catalysts, 9*, Article 346. https://doi.org/10.3390/catal9040346

Hannachi, E., Slimani, Y., Nawaz, M., et al. (2023). Preparation of cerium and yttrium doped ZnO nanoparticles and tracking their structural, optical, and photocatalytic performances. *Journal of Rare Earths, 41*, 682–688. https://doi.org/10.1016/j.jre.2022.03.020

Joshi, S., Srivastava, R. C., & Joshi, A. (2023). Polyaniline/Manganese-Cobalt ferrite nanocomposite as an efficient material for crystal violet dye degradation under sunlight irradiation. *Materials Today Proceedings*. https://doi.org/10.1016/j.matpr.2023.04.462

Jouhannaud, J., Rossignol, J., & Stuerga, D. (2008). Rapid synthesis of tin (IV) oxide nanoparticles by microwave induced thermohydrolysis. *Journal of Solid State Chemistry, 181*, 1439–1444. https://doi.org/10.1016/j.jssc.2008.02.040

Kant, R. (2012). Textile dyeing industry an environmental hazard. *Nature Science (Irvine), 4*, 22–26. https://doi.org/10.4236/ns.2012.41004

Kar, A., Olszówka, J., Sain, S., et al. (2019). Morphological effects on the photocatalytic properties of SnO_2 nanostructures. *Journal of Alloys and Compounds, 810*, 151718. https://doi.org/10.1016/j.jallcom.2019.151718

Karthikeyan, B., & Pandiyarajan, T. (2010). Simple room temperature synthesis and optical studies on Mg doped ZnO nanostructures. *Journal of Luminescence, 130*, 2317–2321. https://doi.org/10.1016/j.jlumin.2010.07.011

Khairy, M., & Zakaria, W. (2014). Effect of metal-doping of TiO_2 nanoparticles on their photocatalytic activities toward removal of organic dyes. *Egyptian Journal of Petroleum, 23*, 419–426. https://doi.org/10.1016/j.ejpe.2014.09.010

Kim, S. P., Choi, M. Y., & Choi, H. C. (2016). Photocatalytic activity of SnO_2 nanoparticles in methylene blue degradation. *Materials Research Bulletin, 74*, 85–89. https://doi.org/10.1016/j.materresbull.2015.10.024

Komal, Srivastava, R. C., Joshi, C. S., & Verma, H. K. (2024). Zinc oxide and nickel ferrite nanocomposite as an efficient photocatalyst for crystal violet dye

degradation. *Solid State Communications, 386*, 115517. https://doi.org/10.1016/j.ssc.2024.115517

Kossar, S., Banu, I. B. S., Aman, N., & Amiruddin, R. (2021). Investigation on photocatalytic degradation of crystal violet dye using bismuth ferrite nanoparticles. *Journal of Dispersion Science and Technology, 42*, 2053–2062. https://doi.org/10.1080/01932691.2020.1806861

Krishnakumar, T., Jayaprakash, R., Parthibavarman, M., et al. (2009). Microwave-assisted synthesis and investigation of SnO_2 nanoparticles. *Materials Letters, 63*, 896–898. https://doi.org/10.1016/j.matlet.2009.01.032

Kumar, S., Bhunia, S., & Ojha, A. K. (2015). Effect of calcination temperature on phase transformation, structural and optical properties of sol-gel derived ZrO_2 nanostructures. *Physica E: Low-dimensional Systems and Nanostructures, 66*, 74–80. https://doi.org/10.1016/j.physe.2014.09.007

Kumar, V. B., Perkas, N., Porat, Z., & Gedanken, A. (2017). Solar-light-driven photocatalytic activity of novel Sn@C-dots-modified TiO_2 catalyst. *ChemistrySelect, 2*, 6683–6688. https://doi.org/10.1002/slct.201701375

Kumari, N., Ghosh, A., Tewari, S., & Bhattacharjee, A. (2014). Synthesis, structural and optical properties of Al doped SnO_2 nanoparticles. *Indian Journal of Physics, 88*, 65–70. https://doi.org/10.1007/s12648-013-0387-0

Lavanya, N., Radhakrishnan, S., & Sekar, C. (2012). Fabrication of hydrogen peroxide biosensor based on Ni doped SnO_2 nanoparticles. *Biosensors and Bioelectronics, 36*, 41–47. https://doi.org/10.1016/j.bios.2012.03.035

Liu, X., Zhang, T., & Zhang, L. (2018). Microwave-induced catalytic application of magnetically separable strontium ferrite in the degradation of organic dyes: Insight into the catalytic mechanism. *Separation and Purification Technology, 195*, 192–198. https://doi.org/10.1016/j.seppur.2017.12.015

Liu, X., Zhang, T., Xu, D., & Zhang, L. (2016). Microwave-assisted catalytic degradation of crystal violet with barium ferrite nanomaterial. *Industrial & Engineering Chemistry Research, 55*, 11869–11877. https://doi.org/10.1021/acs.iecr.6b01762

Madiba, I. G., Émond, N., Chaker, M., et al. (2017). Effects of gamma irradiations on reactive pulsed laser deposited vanadium dioxide thin films. *Applied Surface Science, 411*, 271–278. https://doi.org/10.1016/j.apsusc.2017.03.131

Maleki, A., Safari, M., Shahmoradi, B., et al. (2015). Photocatalytic degradation of humic substances in aqueous solution using Cu-doped ZnO nanoparticles under natural sunlight irradiation. *Environmental Science and Pollution Research, 22*, 16875–16880. https://doi.org/10.1007/s11356-015-4915-7

Manjula, N., & Selvan, G. (2017). Magnetic and antibacterial properties of Zr-doped SnO_2 nanopowders. *Journal of Materials Science: Materials in Electronics, 28*, 15056–15064. https://doi.org/10.1007/s10854-017-7380-x

Mirzayev, M. N., Jabarov, S. H., Asgerov, E. B., et al. (2018). X-ray diffraction and thermodynamics kinetics of SiB_6 under gamma irradiation dose. https://doi.org/10.1007/s12633-018-0039-2

Mohammed Harshulkhan, S., Janaki, K., Velraj, G., et al. (2016). Effect of Ag doping on structural, optical and photocatalytic activity of tungsten oxide (WO_3) nanoparticles. *Journal of Materials Science: Materials in Electronics, 27*, 4744–4751. https://doi.org/10.1007/s10854-016-4354-3

Mohana Priya, S., Geetha, A., & Ramamurthi, K. (2016). Structural, morphological and optical properties of tin oxide nanoparticles synthesized by sol-gel method adding hydrochloric acid. *Journal of Sol-Gel Science and Technology, 78*, 365–372. https://doi.org/10.1007/s10971-016-3966-7

Murugan, R., Kashinath, L., Subash, R., et al. (2018). Pure and alkaline metal ion (Mg, Ca, Sr, Ba) doped cerium oxide nanostructures for photo degradation of methylene blue. *Materials Research Bulletin, 97*, 319–325. https://doi.org/10.1016/j.materresbull.2017.09.026

Nachiar, R. A., & Muthukumaran, S. (2019). Structural, photoluminescence and magnetic properties of Cu-doped SnO_2 nanoparticles co-doped with Co. *Optics and Laser Technology, 112*, 458–466.

https://doi.org/10.1016/j.optlastec.2018.11.055

Nyamukamba, P., Tichagwa, L., Mamphweli, S., & Petrik, L. (2017). Silver/carbon codoped titanium dioxide photocatalyst for improved dye degradation under visible light. *International Journal of Photoenergy, 2017*, Article 3079276. https://doi.org/10.1155/2017/3079276

Pascariu, P., Airinei, A., Olaru, N., et al. (2016). Photocatalytic degradation of Rhodamine B dye using ZnO-SnO_2 electrospun ceramic nanofibers. *Ceramics International, 42*, 6775–6781. https://doi.org/10.1016/j.ceramint.2016.01.054

Patel, A., Soni, S., Mittal, J., et al. (2021). Sequestration of crystal violet from aqueous solution using ash of black turmeric rhizome. *Desalination and Water Treatment, 220*, 342–352. https://doi.org/10.5004/dwt.2021.26911

Patil, G. E., Kajale, D. D., Gaikwad, V. B., & Jain, G. H. (2012). Preparation and characterization of SnO_2 nanoparticles by hydrothermal route. *Materials Letters, 91*, 31–34.

Pradeev raj, K., Sadaiyandi, K., Kennedy, A., et al. (2018). Influence of Mg doping on ZnO nanoparticles for enhanced photocatalytic evaluation and antibacterial analysis. *Nanoscale Research Letters, 13*, Article 2643. https://doi.org/10.1186/s11671-018-2643-x

Rashad, S., Zaki, A. H., & Farghali, A. A. (2019). Morphological effect of titanate nanostructures on the photocatalytic degradation of crystal violet. *Nanomaterials and Nanotechnology, 9*, Article 1778. https://doi.org/10.1177/1847980418821778

Sabri, N. S., Deni, M. S. M., Zakaria, A., & Talari, M. K. (2012). Effect of Mn doping on structural and optical properties of SnO_2 nanoparticles prepared by mechanochemical processing. *Physics Procedia, 25*, 233–239. https://doi.org/10.1016/j.phpro.2012.03.077

Sadhanala, H. K., Senapati, S., Harika, K. V., et al. (2018). Green synthesis of MoS_2 nanoflowers for efficient degradation of methylene blue and crystal violet dyes under natural sunlight conditions. *New Journal of Chemistry, 42*, 14318–14324. https://doi.org/10.1039/c8nj01731j

Sahay, P. P., Mishra, R. K., Pandey, S. N., et al. (2013). Structural, dielectric and photoluminescence properties of co-precipitated Zn-doped SnO_2 nanoparticles. *Current Applied Physics, 13*, 479–486. https://doi.org/10.1016/j.cap.2012.09.010

Sa-nguanprang, S., Phuruangrat, A., Thongtem, T., & Thongtem, S. (2019). Synthesis, analysis, and photocatalysis of Mg-doped ZnO nanoparticles. *Russian Journal of Inorganic Chemistry, 64*, 1841–1848. https://doi.org/10.1134/S0036023619140158

Senthil Kumar, P., Selvakumar, M., Ganesh Babu, S., et al. (2015). CdO nanospheres: Facile synthesis and bandgap modification for superior photocatalytic activity. *Materials Letters, 151*, 45–48. https://doi.org/10.1016/j.matlet.2015.03.047

Sharma, S., Dutta, V., Singh, P., et al. (2019). Carbon quantum dot supported semiconductor photocatalysts for efficient degradation of organic pollutants in water: A review. *Journal of Cleaner Production, 228*, 755–769.

Singh, L. P., Luwang, M. N., & Srivastava, S. K. (2014). Luminescence and photocatalytic studies of Sm^{3+} ion doped SnO_2 nanoparticles. *New Journal of Chemistry, 38*, 115–121. https://doi.org/10.1039/c3nj00759f

Slimani, Y., Almessiere, M. A., Mohamed, M. J. S., et al. (2023). Synthesis of Ce and Sm co-doped TiO_2 nanoparticles with enhanced photocatalytic activity for Rhodamine B dye degradation. *Catalysts, 13*(4), 668. https://doi.org/10.3390/catal13040668

Sudha, A., Maity, T. K., & Sharma, S. L. (2016). Effects of gamma irradiations on structural and electrical properties of indium oxide thin films prepared by thermal evaporation. *Materials Letters, 164*, 372–375. https://doi.org/10.1016/j.matlet.2015.11.003

Tazikeh, S., Akbari, A., Talebi, A., & Talebi, E. (2014). Synthesis and characterization of tin oxide nanoparticles via the co-precipitation method. *Materials Science-Poland, 32*, 98–101. https://doi.org/10.2478/s13536-013-0164-y

Xiong, L., Qin, M., Yang, G., et al. (2016). Performance enhancement of high temperature SnO_2-based planar perovskite solar cells: Electrical characterization and understanding of the mechanism. *Journal of Materials Chemistry A, 4*, 8374–8383. https://doi.org/10.1039/c6ta01839d

Yao, S., Qu, F., Wang, G., & Wu, X. (2017). Facile hydrothermal synthesis of WO_3 nanorods for photocatalysts and supercapacitors. *Journal of Alloys and Compounds, 724*, 695–702. https://doi.org/10.1016/j.jallcom.2017.07.123

Zhang, M., An, T., Hu, X., et al. (2004). Preparation and photocatalytic properties of a nanometer ZnO-SnO_2 coupled oxide. *Applied Catalysis A: General, 260*, 215–222. https://doi.org/10.1016/j.apcata.2003.10.025

Zhou, Q., Chen, W., Xu, L., et al. (2018). Highly sensitive carbon monoxide (CO) gas sensors based on Ni and Zn doped SnO_2 nanomaterials. *Ceramics International, 44*, 4392–4399. https://doi.org/10.1016/j.ceramint.2017.12.038

Peer-review history:
The peer review history for this paper can be accessed here:
https://www.sdiarticle5.com/review-history/122776